

1 Technical Note: Improved partial wavelet coherency for understanding scale-  
2 specific and localized bivariate relationships in geosciences

3 Wei Hu<sup>1</sup> and Bing Si<sup>2</sup>

4 <sup>1</sup>The New Zealand Institute for Plant and Food Research Limited, Private Bag 4704, Christchurch 8140.

5 New Zealand

6 <sup>2</sup>University of Saskatchewan, Department of Soil Science, Saskatoon, SK S7N 5A8, Canada

7 Correspondence to: Wei Hu ([wei.hu@plantandfood.co.nz](mailto:wei.hu@plantandfood.co.nz))

## 8 **Abstract**

9 Bivariate wavelet coherency is a measure of correlation between two variables in the  
10 location-scale (spatial data) or time-frequency (time series) domain. It is particularly suited  
11 to geoscience where relationships between multiple variables differ with locations (times)  
12 and/or scales (frequencies) because of various processes involved. However, it is well-  
13 known that bivariate relationships can be misleading when both variables are dependent on  
14 other variables. Partial wavelet coherency (PWC) has been proposed to detect scale-specific  
15 and localized bivariate relationships by excluding the effects of other variables, but is  
16 limited to one excluding variable and provides no phase information. We aim to develop a  
17 new PWC method that can deal with multiple excluding variables and provide phase  
18 information. Both stationary and non-stationary artificial datasets with the response  
19 variable being the sum of five cosine waves at 256 locations are used to test the method.

20 The new method was also applied to a free water evaporation dataset. Our results verified  
21 the advantages of the new method in capturing phase information and dealing with multiple  
22 excluding variables. Where there is one excluding variable, the new PWC implementation  
23 produces higher and more accurate PWC values than the previously published PWC  
24 implementation that mistakenly considered bivariate real coherence rather than bivariate  
25 complex coherence. We suggest the PWC method is used to untangle scale-specific and  
26 localized bivariate relationships after removing the effects of other variables in geosciences.  
27 The PWC implementations were coded with Matlab and are freely accessible  
28 (<https://figshare.com/s/bc97956f43fe5734c784>).

29

## 30 **1. Introduction**

31 Geoscience data, such as the spatial distribution of soil moisture in undulating terrains  
32 and time series of climatic variables, usually consist of a variety of transient processes with  
33 different scales or frequencies that may be localized in space or time (Torrence and Compo,  
34 1998; Si, 2008; Graf et al., 2014). For example, time series of air temperature usually  
35 fluctuates periodically at different scales (e.g., daily and yearly), but abrupt changes in air  
36 temperature (e.g., extremely high or low) may occur at certain time points as a result of  
37 extreme weather and climate events (e.g., heat and rain). Wavelet methods are widely used  
38 to detect localized features of geoscience data.

39 Wavelet analyses are based on the wavelet transform using mother wavelet function,

40 which expands spatial data (or time series) into location-scale (or time-frequency) space for  
41 identification of localized intermittent scales (or frequencies). For convenience, we will  
42 mainly refer to location and scale irrespective of spatial or time series data unless otherwise  
43 mentioned. Bivariate wavelet coherency (BWC) is widely accepted as a tool for detecting  
44 scale-specific and localized bivariate relationships in a range of areas in geoscience  
45 (Lakshmi et al., 2004; Si and Zeleke, 2005; Das and Mohanty, 2008; Polansky et al., 2010;  
46 Biswas and Si, 2011). The BWC partitions correlation between two variables into different  
47 locations and scales, which are different from the overall relationships at the sampling scale  
48 as shown by the traditional correlation coefficient. For example, BWC analysis indicated  
49 that soil water content of a hummocky landscape in the Canadian Prairies was negatively  
50 correlated to soil organic carbon content at a slope scale (50 m), but they were positively  
51 correlated at a watershed scale (120 m) in summer because of the different processes  
52 involved at different scales (Hu et al., 2017b). Because the positive correlation may cancel  
53 out with the negative one at different scales and/or locations, the traditional correlation  
54 coefficient between soil water content and soil organic carbon content does not differ  
55 significantly from zero, which can be misleading.

56 Recently, Hu and Si (2016) have extended BWC to multiple wavelet coherence (MWC)  
57 that can be used to untangle multivariate ( $\geq 3$  variables) relationships in multiple location-  
58 scale domains. This method has been successfully used in hydrology (Hu et al., 2017b;  
59 Nalley et al., 2019; Su et al., 2019; Gu et al., 2020; Mares et al., 2020) and other areas such  
60 as soil science (Centeno et al., 2020), environmental science (Zhao et al., 2018),  
61 meteorology (Song et al., 2020), and economics (Sen et al., 2019). The MWC application

62 has shown that an increased number of predictor variables does not necessarily explain  
63 more variations in the response variable, partly because predictor variables are usually  
64 cross-correlated (Hu and Si, 2016). For the same reason, bivariate relationships can be  
65 misleading if the predictor variable is correlated with other variables that control the  
66 response variable. Partial correlation analysis is one such method to avoid the misleading  
67 relationships resulting from the interdependence between predictor and other variables  
68 (Kenney and Keeping, 1939). For example, soil water content of the root zone was found  
69 to be positively related to grass yield throughout the year in a small watershed on the  
70 Chinese Loess Plateau (Hu et al., 2017a). This was because higher grass yield usually  
71 coincided with finer soils that usually have higher water holding capacity. After removing  
72 the effects of other factors including sand content, partial correlation analysis indicated that  
73 soil water content was negatively affected by grass yield during growing seasons and not  
74 affected by grass yield during non-growing seasons as expected. The study of Hu et al.  
75 (2017a) clearly demonstrated that partial correlation analysis can be an effective method to  
76 avoid misleading relationships between response (e.g., soil water content) and predictor  
77 variables (e.g., grass yield) when the latter was interdependent with other variables (e.g.,  
78 sand content). However, the extension of partial correlation to the multiple location-scale  
79 domain is limited. In order to better understand the bivariate relationships at various scales  
80 and locations, BWC needs to be extended to partial wavelet coherency (PWC) by  
81 eliminating the effects of other variables.

82 BWC was extended to PWC by Mihanović et al. (2009). Their method has been widely  
83 used in the areas of marine science (Ng and Chan, 2012a, b), meteorology (Tan et al., 2016;

84 Rathinasamy et al., 2017), and economics (Aloui et al., 2018; Altarturi et al., 2018a; Wu et  
85 al., 2020), as well as in the study of greenhouse gas emissions (Jia et al., 2018; Li et al.,  
86 2018; Mutascu and Sokic, 2020), among others. For example, PWC analysis indicated that  
87 the Southern Oscillation Index and Pacific Decadal Oscillation did not affect precipitation  
88 across India, while this was misinterpreted by the BWC analysis because of their  
89 interdependence on Niño 3.4, which affects precipitation (Rathinasamy et al., 2017).  
90 Unfortunately, the PWC implementation in many previous studies (Ng and Chan, 2012b;  
91 Rathinasamy et al., 2017; Aloui et al., 2018; Altarturi et al., 2018b; Jia et al., 2018; Li et al.,  
92 2018; Mutascu and Sokic, 2020; Wu et al., 2020) was based on an incorrect Matlab code  
93 developed by Ng and Chan (2012a) who might have misinterpreted the equation of  
94 Mihanović et al. (2009) and mistakenly used bivariate real coherence rather than bivariate  
95 complex coherence for calculating PWC. Moreover, Mihanović et al. (2009) considered  
96 only one excluding variable (i.e., the variable that influences the response variable is  
97 excluded) and did not include the phase angle difference between response and predictor  
98 variables. The PWC values between response and predictor variables can still be misleading  
99 if more than one variable is interdependent with the predictor variable. This is especially  
100 true if these variables are correlated with the predictor variable at different locations and/or  
101 scales. Without phase information, it is hard to tell if the correlation at a location and scale  
102 is positive or negative.

103 As an extension of previous studies (Mihanović et al., 2009; Hu and Si, 2016), this paper  
104 aims to develop a PWC method that considers more than one excluding variable and  
105 provides phase information. This new method reveals the magnitude and type of bivariate

106 relationships after removing the effects from all potentially interdependent variables. We  
107 expect that the new method produces more accurate PWC values than the implementation  
108 of Ng and Chan (2012a) where there is one excluding variable. The new method is an  
109 extension of the multivariate partial coherency in the frequency (scale) domain (Koopmans,  
110 1995). The proposed method is first tested with artificial datasets following Yan and Gao  
111 (2007) and Hu and Si (2016) to demonstrate its capability of capturing the known  
112 relationships of the artificial data. Then it is applied to a real dataset, i.e., time series of free  
113 water evaporation at the Changwu site in China (Hu and Si, 2016). Finally, the advantages  
114 and weaknesses of the new method are discussed by comparing it with the previous PWC  
115 method (Mihanović et al., 2009) and implementation (Ng and Chan, 2012a).

## 116 **2. Theory**

117 Wavelet analysis is based on the wavelet transform, which includes continuous wavelet  
118 transform and discrete wavelet transform. While the discrete wavelet transform is mainly  
119 used for data compression and noise reduction, the continuous wavelet transform is widely  
120 used for extracting scale-specific and localized features, as in the case of this study  
121 (Grinsted et al., 2004). The wavelet transform decomposes the spatial data (or time series)  
122 into a set of location- and scale-specific wavelet coefficients, which are scaled (contracted  
123 or expanded) and shifted versions of mother wavelets. Different mother wavelets are  
124 available for wavelet transform. Among which, the Morlet wavelet, composed of a complex  
125 exponential multiplied by a Gaussian window, provides a good balance between location  
126 and scale localization. Therefore, continuous wavelet transform with the Morlet wavelet is

127 suitable to transform spatial data (or time series) into a location-scale (or time-frequency)  
128 domain, which allows us to identify both location-specific amplitude and phase information  
129 of wavelet coefficients at different scales (Torrence and Compo, 1998). Wavelet coefficients  
130 and their complex conjugates are used to calculate auto-wavelet power spectra and cross-  
131 wavelet power spectra. BWC is calculated as the ratio of smoothed cross-wavelet power  
132 spectra of two variables to the product of their auto-wavelet power spectra (Grinsted et al.,  
133 2004). Hu and Si (2016) extended wavelet coherence from two to multiple ( $\geq 3$ ) variables  
134 and developed MWC. Detailed information on the calculations of wavelet coefficients,  
135 auto- and cross-wavelet power spectra, BWC, and MWC based on the continuous wavelet  
136 transform can be found in previous studies (e.g., Torrence and Compo, 1998; Grinsted et  
137 al., 2004; Si and Farrell, 2004; Si, 2008; Hu and Si, 2016; Hu et al., 2017b). Here, we will  
138 only introduce the theory and calculation that are most relevant to PWC.

139 Similar to BWC and MWC, PWC is calculated from auto- and cross-wavelet power  
140 spectra, for the response variable  $y$ , predictor variable  $x$ , and excluding variables  $Z$  ( $Z =$   
141  $\{Z_1, Z_2, \dots, Z_q\}$ ). Koopmans (1995) developed the multivariate complex PWC in the  
142 frequency (scale) domain. Here, we extend the Koopmans (1995) method from the  
143 frequency (scale) domain to the time-frequency (location-scale) domain. Therefore, the  
144 complex PWC between  $y$  and  $x$  after excluding variables  $Z$  at scale  $s$  and location  $\tau$ ,  
145  $\gamma_{y,x:Z}(s, \tau)$ , can be written as

$$146 \quad \gamma_{y,x:Z}(s, \tau) = \frac{(1 - R_{y,x,Z}^2(s, \tau)) \gamma_{y,x}(s, \tau)}{\sqrt{(1 - R_{y,Z}^2(s, \tau))(1 - R_{x,Z}^2(s, \tau))}} \quad (1)$$

147 where symbol  $\cdot$  is the notation for excluding variables;  $R_{yx,z}^2(s, \tau)$ ,  $R_{y,z}^2(s, \tau)$ , and  
 148  $R_{x,z}^2(s, \tau)$  can be calculated by following Hu and Si (2016) as

$$149 \quad R_{y,x,z}^2(s, \tau) = \frac{\overleftrightarrow{W}^{y,Z}(s, \tau) \overleftrightarrow{W}^{Z,Z}(s, \tau)^{-1} \overleftrightarrow{W}^{x,Z}(s, \tau)}{\overleftrightarrow{W}^{y,x}(s, \tau)} \quad (2)$$

$$150 \quad R_{y,z}^2(s, \tau) = \frac{\overleftrightarrow{W}^{y,Z}(s, \tau) \overleftrightarrow{W}^{Z,Z}(s, \tau)^{-1} \overleftrightarrow{W}^{y,Z}(s, \tau)}{\overleftrightarrow{W}^{y,y}(s, \tau)} \quad (3)$$

$$151 \quad R_{x,z}^2(s, \tau) = \frac{\overleftrightarrow{W}^{x,Z}(s, \tau) \overleftrightarrow{W}^{Z,Z}(s, \tau)^{-1} \overleftrightarrow{W}^{x,Z}(s, \tau)}{\overleftrightarrow{W}^{x,x}(s, \tau)} \quad (4)$$

152 Eq. (1) can be also derived analogously from the complex partial spectrum for the frequency  
 153 domain according to the definition of complex coherence between two variables in the time-  
 154 frequency domain (see the Supplement (Sect. S1) for the derivation process). Note that  
 155  $R_{y,x,z}^2(s, \tau)$  is a matrix with complex values, while  $R_{y,z}^2(s, \tau)$  and  $R_{x,z}^2(s, \tau)$  are matrices  
 156 with real numbers.  $\gamma_{y,x}(s, \tau)$  is the complex wavelet coherence between  $y$  and  $x$ , which  
 157 can be written as

$$158 \quad \gamma_{y,x}(s, \tau) = \frac{\overleftrightarrow{W}^{y,x}(s, \tau)}{\left( \overleftrightarrow{W}^{y,y}(s, \tau) \overleftrightarrow{W}^{x,x}(s, \tau) \right)^{1/2}} \quad (5)$$

159 where  $\overleftrightarrow{(\ )}$  is the smoothing operator,  $\overline{(\ )}$  is the complex conjugate operator,  $(\ )^{-1}$   
 160 indicates the inverse of the matrix, and

$$161 \quad \overleftrightarrow{W}^{y,Z}(s, \tau) = \left[ \overleftrightarrow{W}^{y,Z_1}(s, \tau) \overleftrightarrow{W}^{y,Z_2}(s, \tau) \dots \overleftrightarrow{W}^{y,Z_q}(s, \tau) \right] \quad (6)$$

$$162 \quad \overleftrightarrow{W}^{x,Z}(s, \tau) = \left[ \overleftrightarrow{W}^{x,Z_1}(s, \tau) \overleftrightarrow{W}^{x,Z_2}(s, \tau) \dots \overleftrightarrow{W}^{x,Z_q}(s, \tau) \right] \quad (7)$$



$$163 \quad \leftrightarrow_W^{Z,Z}(s, \tau) = \begin{bmatrix} \leftrightarrow_W^{Z_1, Z_1}(s, \tau) & \cdots & \leftrightarrow_W^{Z_1, Z_q}(s, \tau) \\ \vdots & \ddots & \vdots \\ \leftrightarrow_W^{Z_q, Z_1}(s, \tau) & \cdots & \leftrightarrow_W^{Z_q, Z_q}(s, \tau) \end{bmatrix} \quad (8)$$

164 where  $\leftrightarrow_W^{A,B}(s, \tau)$  is the smoothed auto-wavelet power spectra (when  $A=B$ ) or cross-  
165 wavelet power spectra (when  $A \neq B$ ) at scale  $s$  and location  $\tau$ , respectively.

166 The squared PWC (hereinafter referred to as PWC) at scale  $s$  and location  $\tau$ ,  $\rho_{y,x,Z}^2$ , can  
167 be written as

$$168 \quad \rho_{y,x,Z}^2 = \frac{|1 - R_{y,x,Z}^2(s, \tau)|^2 R_{y,x}^2(s, \tau)}{(1 - R_{y,Z}^2(s, \tau))(1 - R_{x,Z}^2(s, \tau))} \quad (9)$$

169 where  $R_{y,x}^2(s, \tau)$  is squared BWC between  $y$  and  $x$ , which can be expressed as

$$170 \quad R_{y,x}^2(s, \tau) = \frac{\overleftrightarrow_W^{y,x}(s, \tau) \overleftrightarrow_W^{y,x}(s, \tau)}{\overleftrightarrow_W^{y,y}(s, \tau) \overleftrightarrow_W^{x,x}(s, \tau)} \quad (10)$$

171 The phase angle (i.e., angle between two complex numbers) between  $y$  and  $x$  after  
172 excluding effect of  $Z$  is

$$173 \quad \vartheta_{y,x,Z}(s, \tau) = \varphi_{y,x,Z}(s, \tau) + \vartheta_{y,x}(s, \tau) \quad (11)$$

174 where

$$175 \quad \varphi_{y,x,Z}(s, \tau) = \arg(1 - R_{y,x,Z}^2(s, \tau)) \quad (12)$$

176 and  $\vartheta_{y,x}(s, \tau)$  is the wavelet phase between  $y$  and  $x$ , which can be expressed as

$$177 \quad \vartheta_{y,x}(s, \tau) = \tan^{-1}(\text{Im}(W^{y,x}(s, \tau)) / \text{Re}(W^{y,x}(s, \tau))) \quad (13)$$

178 where  $\arg$  denotes the argument of the complex number,  $W^{y,x}(s, \tau)$  is the cross-wavelet

179 power spectrum between  $y$  and  $x$  at scale  $s$  and location  $\tau$ ; Im and Re denote the  
180 imaginary and real part of  $W^{y,x}(s, \tau)$ , respectively.

181 When only one variable (e.g.,  $Z_1$ ) is excluded, Eq.(9) can be written as (see the  
182 Supplement (Sect. S2) for the derivation process)

$$183 \quad \rho_{y,x \cdot Z_1}^2 = \frac{|\gamma_{y,x}(s,\tau) - \gamma_{y,Z_1}(s,\tau)\overline{\gamma_{x,Z_1}(s,\tau)}|^2}{(1-R_{y,Z_1}^2(s,\tau))(1-R_{x,Z_1}^2(s,\tau))} \quad (14)$$

184 The widely used Monte Carlo method (Torrence and Compo, 1998; Grinsted et al., 2004;  
185 Si and Farrell, 2004) is used to calculate PWC at the 95% confidence level. In brief, the  
186 PWC calculation is repeated for a sufficient number (i.e., minimum number required) of  
187 times using data generated by Monte Carlo simulations based on the first-order  
188 autocorrelation coefficient ( $r_1$ ). The first-order autoregressive model (AR(1)) is chosen  
189 because most geoscience data can be effectively simulated by it (Wendroth et al., 1992;  
190 Grinsted et al., 2004; Si and Farrell, 2004), although we recognize that time series with  
191 long-range dependence is also common in many areas such as hydrology (Szolgayová et  
192 al., 2014). Different combinations of  $r_1$  values (i.e., 0.0, 0.5, and 0.9) were used to generate  
193 10 to 10 000 AR(1) series with three, four and five variables. Our results indicate that the  
194 noise combination has little impact on the PWC values at the 95% confidence level as also  
195 found by Grinsted et al. (2004) for the BWC case (data not shown). The relative difference  
196 of PWC at the 95% confidence level compared with that calculated from the 10 000 AR(1)  
197 series decreases with the increase in number of AR(1) series (Fig. S1 of Sect. S3 in the  
198 Supplement). When the number of AR(1) is above 300, a very low maximum relative

199 difference (e.g., <2%) is observed. Therefore, a repeating number of 300 seems to be  
 200 sufficient for a significance test. However, if calculation time is not a barrier, a higher  
 201 repeating number, such as  $\geq 1000$ , is recommended. The 95<sup>th</sup> percentile of PWCs of all  
 202 simulations at each scale represents PWC at the 95% confidence level. The average PWC,  
 203 percent area of significant coherence (PASC) relative to the whole wavelet location–scale  
 204 domain (Hu and Si, 2016), and average value of significant PWC (PWC<sub>sig</sub>) are also  
 205 calculated for different location–scale domains.

206 In the case of one excluding variable ( $Z = \{Z_1\}$ ), Mihanović et al. (2009) suggested that  
 207 PWC can be calculated by an equation analogous to the traditional partial correlation  
 208 squared (Kenney and Keeping, 1939) without giving detailed derivation process. Their  
 209 equation is the same as Eq. (14). Unfortunately, Ng and Chan (2012a) might have  
 210 misinterpreted the equation of Mihanović et al. (2009) and developed Matlab code for  
 211 calculating PWC using the equation expressed as

$$212 \quad \rho_{y,x;Z_1}^2 = \frac{|R_{y,x}(s,\tau) - R_{y,Z_1}(s,\tau) R_{x,Z_1}(s,\tau)|^2}{(1 - R_{y,Z_1}^2(s,\tau))(1 - R_{x,Z_1}^2(s,\tau))} \quad (15)$$

213 where  $R_{y,x}(s, \tau)$ ,  $R_{y,Z_1}(s, \tau)$ , and  $R_{x,Z_1}(s, \tau)$  are the square root of  $R_{y,x}^2(s, \tau)$ ,  $R_{y,Z_1}^2(s, \tau)$ ,  
 214  $R_{x,Z_1}^2(s, \tau)$ , respectively.  $R_{y,Z_1}^2(s, \tau)$  and  $R_{x,Z_1}^2(s, \tau)$  can be calculated from Eq. (10) by  
 215 replacing  $y$  and  $x$  with their corresponding variables. Eq. (15) has been widely used to  
 216 calculate PWC in the case of one excluding variable (Ng and Chan, 2012b; Rathinasamy et  
 217 al., 2017; Aloui et al., 2018; Altarturi et al., 2018b; Jia et al., 2018; Li et al., 2018; Mutascu  
 218 and Sokic, 2020; Wu et al., 2020). Note that complex coherence and real coherence are

219 involved in the numerators of Eqs. (14) and (15), respectively, while the denominators are  
220 exactly the same. Further comparison indicates that Eq. (15) underestimates PWC value  
221 relative to Eq. (14) unless  $\gamma_{y,x}(s, \tau)$  and  $\gamma_{y,z_1}(s, \tau) \overline{\gamma_{x,z_1}(s, \tau)}$  in Eq. (14) are collinear  
222 (i.e., their arguments are identical) under which the two equations produce the same PWC  
223 values. Differences between Eqs. (14) and (15) will be discussed further using both artificial  
224 data and a real dataset. For comparison purposes, we refer to Eqs. (14) and (15) as the new  
225 implementation and the classical implementation, respectively.

### 226 **3. Method test using artificial data**

#### 227 **3.1 Artificial data and analysis**

228 PWC is first tested using the cosine-like artificial dataset produced following Yan and  
229 Gao (2007). The cosine-like artificial datasets are suitable for testing the new method  
230 because they mimic many spatial or time series data in geoscience such as climatic variables,  
231 hydrologic fluxes, seismic signals, El Niño-Southern Oscillation, land surface topography,  
232 ocean waves, and soil moisture. The procedures to test PWC are largely based on Hu and  
233 Si (2016), where the same dataset has been used to test the MWC method (refer to Hu and  
234 Si (2016) for a detailed description of the artificial dataset). The response variable ( $y$  and  $z$   
235 for the stationary and non-stationary case, respectively) is the sum of five cosine waves ( $y_1$   
236 to  $y_5$  and  $z_1$  to  $z_5$  for the stationary and non-stationary case, respectively) at 256 locations  
237 (Hu and Si, 2016). For  $y_1$  to  $y_5$ , they have consistent dimensionless scales of 4, 8, 16, 32,  
238 and 64, respectively, across the series. From  $z_1$  to  $z_5$ , the dimensionless scales gradually  
239 change with location, with the maximum dimensionless scales of 4, 8, 16, 32, and 64,

240 respectively. The variance of the response variable  $y$  and  $z$  is 2.5. All other variables are  
241 orthogonal to each other with equal variance of 0.5. The predictor and excluding variables  
242 (Fig. S1 of Sect. S4 in the Supplement) are selected from two of the five cosine waves (i.e.,  
243  $y_2$  and  $y_4$  or  $z_2$  and  $z_4$ ) and/or their derivatives. The exact variables and procedures to test  
244 the new PWC method are explained below.

245 First, PWC between response variable  $y$  (or  $z$ ) and predictor variable, i.e.,  $y_2$  (or  $z_2$ ), is  
246 calculated after excluding the effect of one variable. Four types of excluding variable are  
247 involved (Fig. S2 of Sect. S4 in the Supplement): (a) original series of  $y_4$  (or  $z_4$ ); (b) second  
248 half of the original series of  $y_2$  (or  $z_2$ ) are replaced by 0 to simulate abrupt changes (i.e.,  
249 transient and localized feature) of the spatial data. They are referred to as  $y_{2,h0}$  (or  $z_{2,h0}$ ); (c)  
250 white noises with zero-mean and standard deviations of 0.3 (weak noise), 1 (moderate  
251 noise), and 4 (high noise) are added to  $y_2$  (or  $z_2$ ) as suggested by Hu and Si (2016) to  
252 simulate non-perfect cyclic patterns of the excluding variables. They are referred to as  $y_{2,w}$   
253 (or  $z_{2,w}$ ),  $y_{2,m}$  (or  $z_{2,m}$ ), and  $y_{2,s}$  (or  $z_{2,s}$ ), respectively; and (d) a combination of type b and  
254 type c. They are referred to as  $y_{2,w,h0}$  (or  $z_{2,w,h0}$ ),  $y_{2,m,h0}$  (or  $z_{2,m,h0}$ ), and  $y_{2,s,h0}$  (or  $z_{2,s,h0}$ ),  
255 respectively.

256 Second, PWC between response variable  $y$  (or  $z$ ) and predictor variable, i.e.,  $y_{24}$  (sum of  
257  $y_2$  and  $y_4$ ) for the stationary case or  $z_{24}$  (sum of  $z_2$  and  $z_4$ ) for the non-stationary case, is  
258 calculated with two excluding variables, which is a combination of  $y_4$  (or  $z_4$ ) and  $y_2$  (or  $z_2$ )  
259 or its noised series ( $y_{2,w}$  or  $z_{2,w}$ ,  $y_{2,m}$  or  $z_{2,m}$ , and  $y_{2,s}$  or  $z_{2,s}$ ).

260 The merit of the artificial data is that we know the exact scale-specific and localized

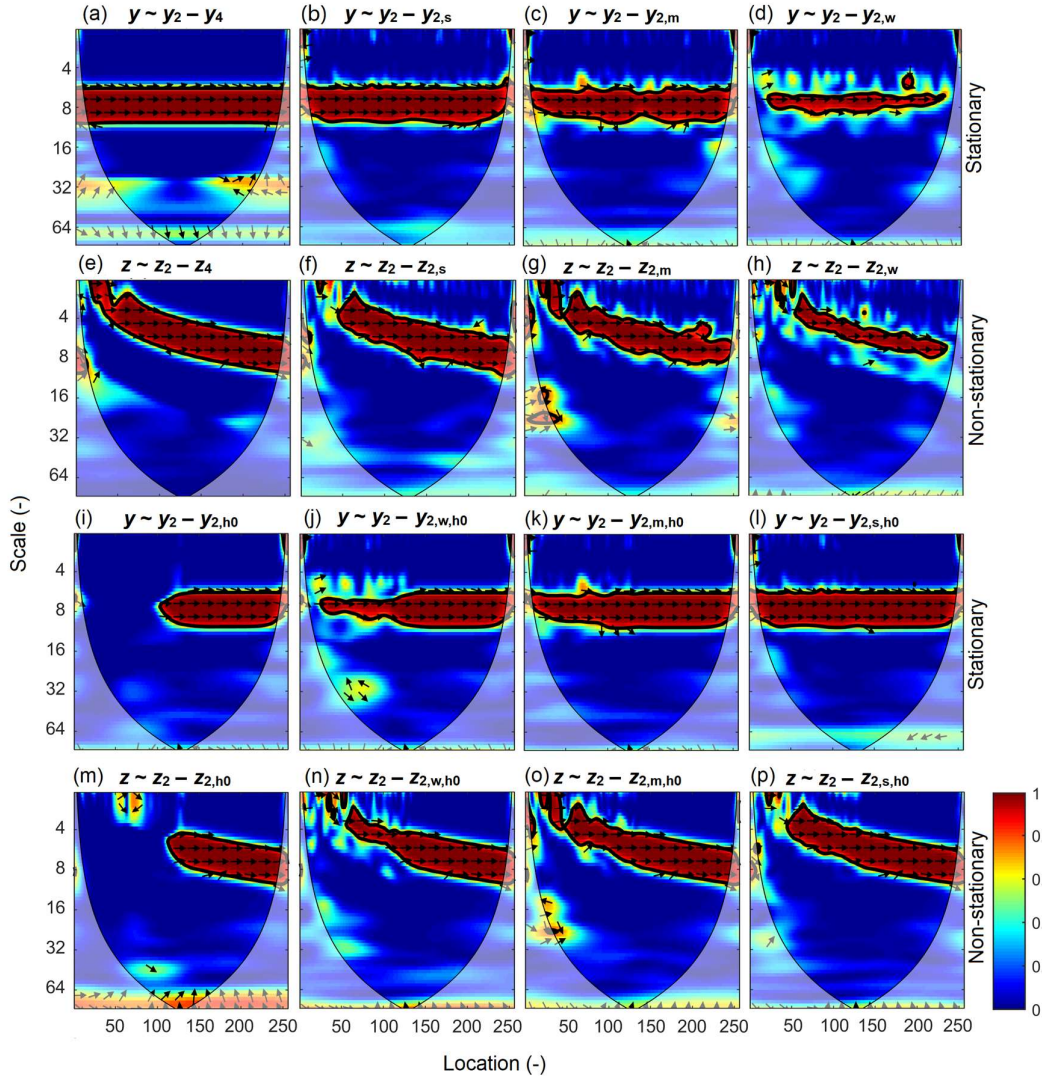
261 bivariate relationships after the effect of excluding variables is removed. Theoretically, we  
262 expect (a) PWC is 1 at scales corresponding to relative complement of excluding variable  
263 scales in predictor variable scales, and 0 at other scales. For example, PWC between  $y$  and  
264  $y_{24}$  after excluding the effect of  $y_4$  is expected to be 1 at the scale of 8, which is the relative  
265 complement of scale of excluding variable  $y_4$  (32) in scales of predictor variable  $y_{24}$  (8 and  
266 32), and 0 at other scales; (b) PWC remains 1 at the second half of series where spatial  
267 series is replaced by 0, and 0 at the first half of the original series. For example, PWC  
268 between  $y$  and  $y_2$  after excluding the effect of  $y_{2,h0}$  is expected to be 0 and 1 at the first and  
269 second half of series, respectively, at the scale of 8; and (c) PWC increases as more noises  
270 are included in the excluding variables. For example, PWC between  $y$  and  $y_2$  after excluding  
271 the effect of noised series of  $y_2$  is expected to increase with increasing noises in an order of  
272  $y_{2,s} > y_{2,m} > y_{2,w}$  at the scale of 8.

### 273 **3.2 PWC with artificial data**

#### 274 3.2.1 PWC with one excluding variable using the new method

275 Fig. 1 shows PWC between response variable  $y$  (or  $z$ ) and predictor variable  $y_2$  (or  $z_2$ ) by  
276 excluding one variable. For the stationary case, there is one horizontal band (red color)  
277 representing an in-phase high PWC value at scales around 8 for all locations after  
278 eliminating the effect of  $y_4$  (Fig. 1a). Note that the PWC values between  $y$  and  $y_2$  after  
279 excluding the effect of  $y_4$  are not exactly 1 as would be expected at all location-scale  
280 domains, because of the effect of smoothing along locations and scales. However, the PWC  
281 values at the center of the significance band, which corresponds to the predictor variable  $y_2$

282 at exactly the scale of 8, are very close to 1 (0.996), and the mean  $PWC_{sig}$  values are very  
 283 high (i.e., 0.96). The result is similar to the BWC between  $y$  and  $y_2$  (data not shown). This  
 284 is understandable because  $y_4$  is orthogonal to  $y_2$ , and excluding the effect of  $y_4$  does not  
 285 affect the relationship between  $y$  and  $y_2$  at all.



286

287 **Figure 1.**

288 Partial wavelet coherence (PWC) between response variable  $y$  (or  $z$ ) and predictor variable  
 289  $y_2$  (or  $z_2$ ) after excluding the effect of variables  $y_4$  (or  $z_4$ ),  $y_{2,s}$  (or  $z_{2,s}$ ),  $y_{2,m}$  (or  $z_{2,m}$ ),  $y_{2,w}$  (or  
 290  $z_{2,w}$ ),  $y_{2,h0}$  (or  $z_{2,h0}$ ),  $y_{2,w,h0}$  (or  $z_{2,w,h0}$ ),  $y_{2,m,h0}$  (or  $z_{2,m,h0}$ ), and  $y_{2,s,h0}$  (or  $z_{2,s,h0}$ ) for the stationary

291 (or non-stationary) case using the new method. Arrows represent the phase angles of the  
292 cross-wavelet power spectra between two variables after eliminating the effect of excluding  
293 variables. Arrows pointing to the right (left) indicate positive (negative) correlations. Thin  
294 and thick solid lines show the cones of influence and the 95% confidence levels,  
295 respectively. All variables were generated by following Yan and Gao (2007) and Hu and Si  
296 (2016) and are explained in Section 3.1 and shown in Fig. S2 of Sect. S3 in the Supplement.

297 Compared with the case of excluding variable of  $y_4$  (Fig. 1a), excluding the effect of  $y_{2,s}$   
298 (Fig. 1b) results in slightly narrower band of significant PWC and slightly reduced mean  
299  $PWC_{sig}$  (0.94 versus 0.96). When less noise is included in the excluding variables (i.e.,  $y_{2,m}$   
300 and  $y_{2,w}$ ) (Fig. 1c-d), the significant PWC band becomes narrower. The PASC values are  
301 86%, 77%, and 32% for excluding  $y_{2,s}$ ,  $y_{2,m}$  and  $y_{2,w}$ , respectively, at scales of 6–10.  
302 Moreover, the mean  $PWC_{sig}$  decreases from 0.94 ( $y_{2,s}$ ) to 0.93 ( $y_{2,m}$ ) and 0.89 ( $y_{2,w}$ ) when  
303 progressively less noise is added (Fig. 1b-d). For the non-stationary case, similar results are  
304 obtained (Fig. 1e-h). The only difference is that the scales with significant PWC values  
305 change with location, as is found for MWC (Hu and Si, 2016).

306 When the second half of the excluding variable series is replaced by 0, the PWC values  
307 in that half are close to 1, while those in the first half of data series are 0 at scales  
308 corresponding to the predictor variable (Fig. 1i and 1m). For the stationary case, after  
309 excluding the effect of  $y_{2,h0}$ , the PWC values are close to 1 (0.98) and 0 in the second and  
310 first half of the data series, respectively, at the dimensionless scale of 8 (Fig. 1i). Similar  
311 results are observed for the non-stationary case (Fig. 1m). This is anticipated because the  
312 series of 0s is independent of the predictor variable and hence has no effect on the  
313 correlations between response and predictor variables at these locations. If different

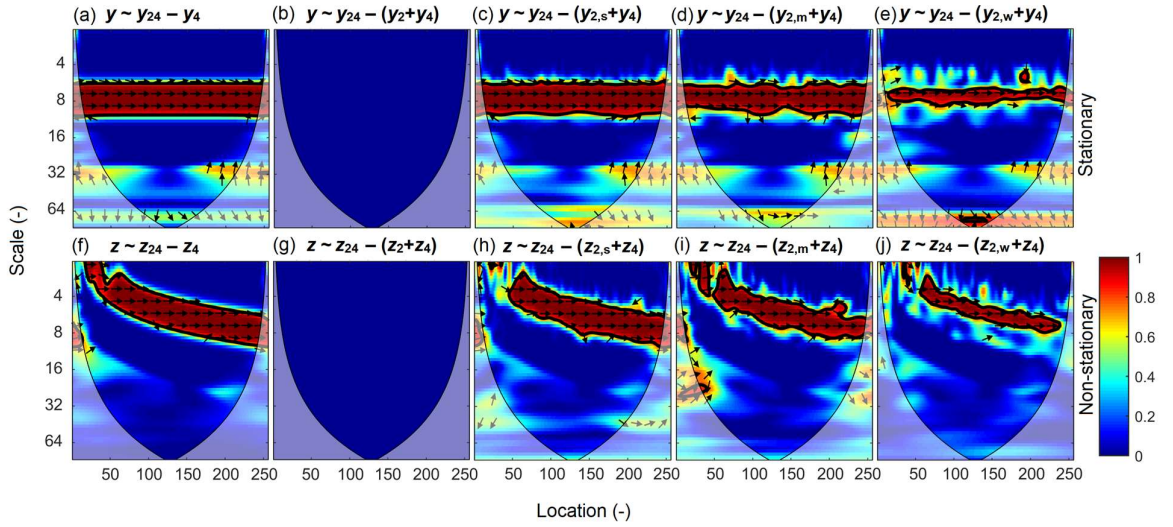


314 magnitudes of noises are added to the first half of the excluding variables ( $y_2$  or  $z_2$ ), the  
315 significant PWC band in the first half becomes wider as the magnitude of noises increases,  
316 while the significant PWC band in the second half remains almost unchanged (Fig. 1j-l and  
317 Fig. 1n-p). In the stationary case, for example, the PASC values at scales of 6–10 are 40%  
318 ( $y_{2,w,h0}$ ), 74% ( $y_{2,m,h0}$ ), and 86% ( $y_{2,s,h0}$ ) in the first half, while those values vary from 86%  
319 to 90% in the second half (Fig. 1j-l). Meanwhile, the mean  $PWC_{sig}$  in the first half at scales  
320 of 6–10 increases from 0.91 to 0.94 in both the stationary (Fig. 1j-l) and non-stationary (Fig.  
321 1n-p) cases as more noises are added to the excluding variable  $y_2$  or  $z_2$ . This indicates that  
322 the new PWC method can also capture the abrupt changes (Fig. 1i and 1m) in the data series,  
323 and has the ability to deal with localized relationships.

### 324 3.2.2 PWC with two excluding variables using the new method

325 When both  $y_2$  and  $y_4$  (or  $z_2$  and  $z_4$ ) are considered in the predictor variables, there are two  
326 bands of wavelet coherence of 1 between  $y$  (or  $z$ ) and  $y_{24}$  (or  $z_{24}$ ) (Hu and Si, 2016), which  
327 correspond to the scales of two predictor variables. However, after the effect of  $y_4$  (or  $z_4$ ) is  
328 removed, only one band with PWC of around 1 occurs at the scale of the predictor variable  
329  $y_2$  (or  $z_2$ ) (Fig. 2a and 2f). After both predictor variables  $y_2$  and  $y_4$  (or  $z_2$  and  $z_4$ ) are excluded  
330 (Fig. 2b and 2g), PWC between  $y$  (or  $z$ ) and  $y_{24}$  (or  $z_{24}$ ) is 0 at all location-scale domains as  
331 expected. When one of the excluding variables  $y_2$  (or  $z_2$ ) is added with noises, the  
332 relationship between response variable  $y$  (or  $z$ ) and predictor variable  $y_{24}$  (or  $z_{24}$ ) becomes  
333 significant at scales of the excluding variable  $y_2$  (or  $z_2$ ) (Fig. 2c and 2h). Similar to the case  
334 of one excluding variable (Fig. 1), less noise in the excluding variable of  $y_2$  (or  $z_2$ ) results

335 in a narrower significant PWC band, and reduced mean  $PWC_{sig}$  values, e.g., from 0.96 ( $y_{2,s}$ )  
 336 to 0.90 ( $y_{2,w}$ ) in the stationary case (Fig. 2c-e) and from 0.95 ( $z_{2,s}$ ) to 0.92 ( $z_{2,w}$ ) in the non-  
 337 stationary case (Fig. 2h-j).



338

339 **Figure 2.**

340 Partial wavelet coherency (PWC) between response variable  $y$  (or  $z$ ) and predictor variable  
 341  $y_{24}$  (or  $z_{24}$ ) after excluding the effect of variables  $y_4$  (or  $z_4$ ),  $y_2+y_4$  (or  $z_2+z_4$ ),  $y_{2,s}+y_4$  (or  $z_{2,s}+z_4$ ),  
 342  $y_{2,m}+y_4$  (or  $z_{2,m}+z_4$ ), and  $y_{2,w}+y_4$  (or  $z_{2,w}+z_4$ ) for the stationary (or non-stationary) case using  
 343 the new method. All variables were generated by following Yan and Gao (2007) and Hu  
 344 and Si (2016) and are explained in Sect. 3.1 and shown in Fig. S2 of Sect. S3 in the  
 345 Supplement.

## 346 4. Method application with real dataset

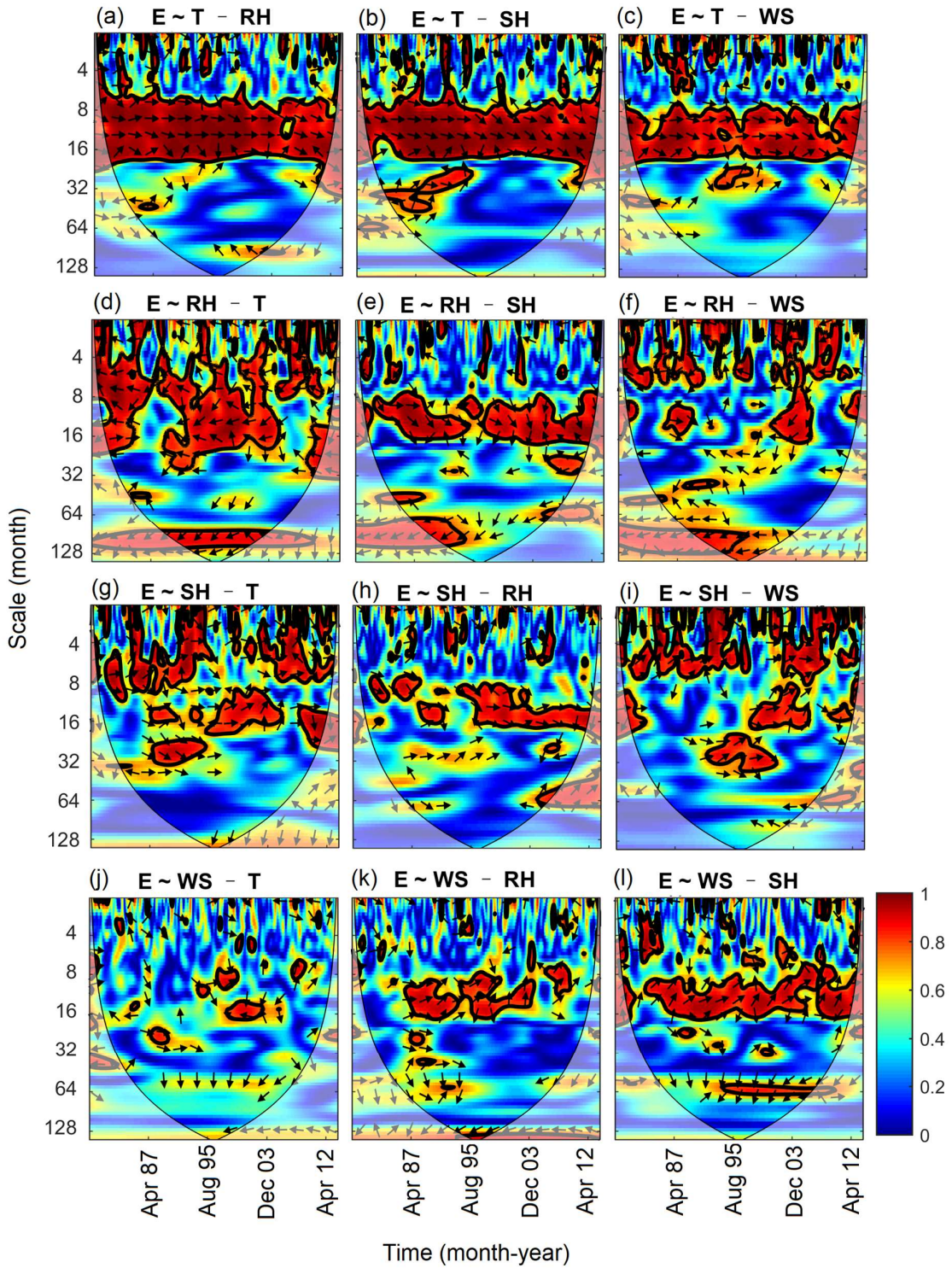
### 347 4.1 Description of free water evaporation dataset

348 The free water evaporation dataset was used to test MWC (Hu and Si, 2016). In brief,  
 349 this dataset includes monthly free water evaporation (E), mean temperature (T), relative

350 humidity (RH), sun hours (SH), and wind speed (WS) between January 1979 and December  
351 2013 at Changwu site in Shaanxi province provided by the China Meteorological  
352 Administration. During this period, the average daily temperature was 9.4 °C, the average  
353 annual rainfall was 571 mm and annual potential evapotranspiration was 883 mm. Because  
354 of its location between semi-arid and subhumid climates, agricultural production at the  
355 Changwu site is constrained by water availability. Results of wavelet power spectrum of E  
356 and BWC between every two variables are shown in Fig. S3 and Fig. S4 (Sect. S3 in the  
357 Supplement), respectively.

#### 358 **4.2 PWC with free water evaporation dataset**

359 The PWC analysis indicates that the correlations between E and T after excluding the  
360 effect of each of other three variables (RH, SH, and WS) were almost the same as those  
361 indicated by BWC (Fig. 3a-c and Fig. S4 of Sect. S3 in the Supplement). For example, E  
362 and T, after excluding the effect of RH, were positively correlated at the medium scales (8–  
363 32 months). The PASC was 61% and mean  $PWC_{sig}$  value was 0.94. No significant  
364 correlations between E and T from 1979 to 1992 were found at scales around 64 months  
365 after eliminating the influence of RH (Fig. 3a-c). This implies that the influence of mean  
366 temperature on E at these scales and years may be associated with the negative influence of  
367 RH on both E and T (Fig. S4 of Sect. S3 in the Supplement).



368

369 **Figure 3.**

370 Partial wavelet coherency (PWC) between evaporation (E) and each meteorological factor

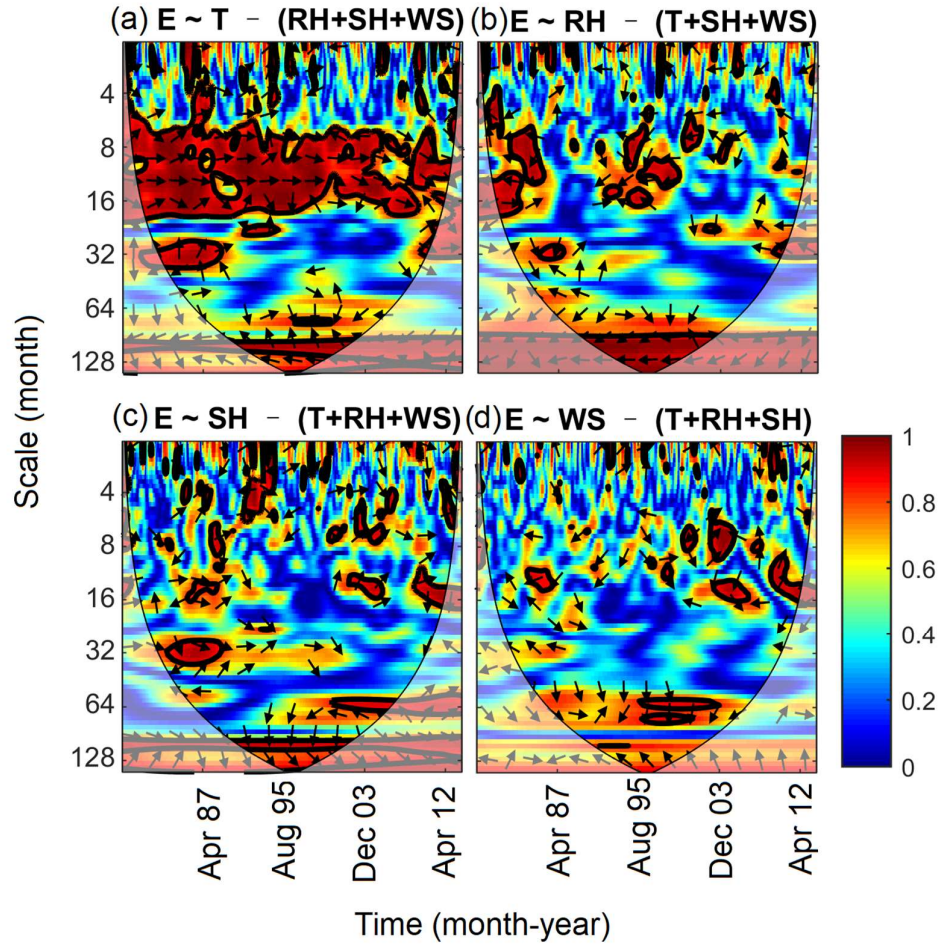
371 (T, mean temperature; RH, relative humidity; SH, sun hours; WS, wind speed) after  
372 excluding the effect of each of other three meteorological factors.

373 PWC between E and RH depended on the excluding variable and scale (Fig. 3d-f). The  
374 mean PWC and PASC between E and RH after excluding T were 0.60 and 34%, respectively,  
375 which are comparable with the mean BWC (0.62) and PASC (40%) between E and RH.  
376 The corresponding values after excluding SH and WS were 0.50 and 0.53 (PWC), 22% and  
377 21% (PASC), respectively. In addition, compared with the BWC between E and RH (Fig.  
378 S4 of Sect. S3 in the Supplement), correlations between E and RH were weak at small scales  
379 (<8 months) and medium scales (8–32 months) after eliminating the influence of SH and  
380 WS (Fig. 3e-f), respectively. Therefore, excluding the variable of T had less influence on  
381 the coherence between E and RH compared with excluding the variables of SH and WS.  
382 This is mainly because RH and T are correlated with E at different scales (Fig. S4 of Sect.  
383 S3 in the Supplement), i.e., mean temperature affected E mainly at medium scales, while  
384 RH affected E across all scales. However, the domain where SH and WS were correlated  
385 with E was a subset of that where RH and E were correlated (Fig. S4 of Sect. S3 in the  
386 Supplement).

387 The relationships between E and SH after excluding the other three factors were less  
388 consistent (Fig. 3g-h). The areas with significant corrections were scattered over the whole  
389 location-scale domain but differed with excluding factor. The PASC varied from 12%  
390 (excluding RH) to 20% (excluding T and WS), which is much lower than the PASC (28%)  
391 in the case of BWC. The significant relationships between E and WS were only limited to  
392 very small areas except for the case of SH being excluded, where E and WS were positively

393 correlated at scales of 8–16 months most of the time (Fig. 3j-l).

394 In general, the PASC decreased after excluding the effects of more factors (data not  
395 shown). The correlations between E and each variable after eliminating the effects of all  
396 other variables are shown in Fig. 4. The correlations between E and T were still significant  
397 at the medium scales (8–32 months) (Fig. 4a), where PASC value was 52% with mean  
398  $PWC_{sig}$  of 0.92. The E was still correlated with RH at large scales (>85 months) (Fig. 4b),  
399 where PASC value was 35% with mean  $PWC_{sig}$  of 0.96. Interestingly, the domain with  
400 significant correlation between E and SH and WS was very limited (Fig. 4c-d). This  
401 indicates that the influences of SH and WS on E have already been covered by RH and T.  
402 This is in agreement with the MWC results that RH and T were the best to explain E  
403 variations at all scales (Hu and Si, 2016). Although the RH had the greatest mean wavelet  
404 coherence and PASC at the entire location-scale domains, the PWC analysis seems to  
405 support that mean temperature was the most dominating factor for free water evaporation  
406 at the 1-year cycle (8–16 months), which is the dominant scale of E variation (Fig. S3 of  
407 Sect. S3 in the Supplement).



408

409 **Figure 4.**

410 Partial wavelet coherency (PWC) between evaporation (E) and each meteorological factor  
 411 (T, mean temperature; RH, relative humidity; SH, sun hours; WS, wind speed) after  
 412 excluding the effects of all other three factors.

413 **5. Discussion on the advantages and weaknesses of the new method**

414 **5.1 Advantages**

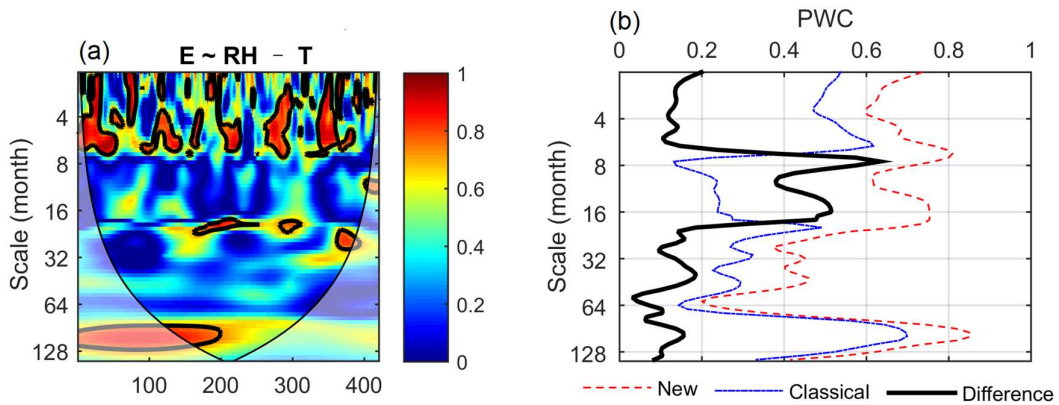
415 We extend the partial coherence method from the frequency (scale) domain (Koopmans,  
 416 1995) to the time-frequency (location-scale) domain. The new method is an extension of

417 previous work on PWC and MWC (Mihanović et al., 2009; Hu and Si, 2016). The method  
418 test and application have verified that it has the advantage of dealing with more than one  
419 excluding variable and providing the phase information associated with PWC. In the case  
420 of one excluding variable, Mihanović et al. (2009) has suggested to calculate PWC by using  
421 an equation analogous to the traditional partial correlation squared (Eq. 14), which can be  
422 derived from our Eq. (9). However, their equation was, unfortunately, widely used by  
423 replacing the complex coherence in Eq. (14) with real coherence as expressed in Eq. (15)  
424 (Ng and Chan, 2012b, a; Rathinasamy et al., 2017; Aloui et al., 2018; Altarturi et al., 2018b;  
425 Jia et al., 2018; Li et al., 2018; Mutascu and Sokic, 2020; Wu et al., 2020). This mistake is  
426 corrected in this paper.

427 The differences between the new (Eq.14) and the classical implementation (Eq. 15) are  
428 compared in the case of one excluding variable using both the artificial and real datasets.  
429 Except for the phase information, the two implementations generally produce comparable  
430 coherence for the artificial dataset (Fig. S5 of Sect. S3 in the Supplement). However, the  
431 new implementation produces consistently and slightly higher coherence than the classical  
432 implementation. For example, their mean PWCs between  $y$  and  $y_2$  at the scale of 8 after  
433 excluding the effect of  $y_4$  are 1.00 and 0.97, respectively. This indicates that the new  
434 implementation produces coherence between  $y$  and  $y_2$  at the scale (8) of  $y_2$  closer to 1 as we  
435 expect. While the classical implementation produces similar PWC between E and other  
436 meteorological factors in most cases especially for the coherence between E and T after  
437 excluding the effects of others (Fig. S6 of Sect. S3 in the Supplement), large differences  
438 between these two implementations can also be observed. For example, while the new



439 implementation recognizes the strong coherence between E and RH after excluding the  
 440 effect of T at scales of around 1 year (Fig. 3d), this coherence was negligible by the classical  
 441 implementation (Fig. 5a). Mean PWC values by the new implementation were consistently  
 442 higher than the classical implementation, and the differences ranged from 0.4 to 0.6 around  
 443 the scale of 1 year (Fig. 5b). Considering the real coherence (Eq.15) rather than complex  
 444 coherence (Eq.14) between every two variables in the numerators can potentially result in  
 445 large underestimation of the partial wavelet coherence. Therefore, the ability of the new  
 446 method and implementation to produce more accurate results than the classical  
 447 implementation is one of its advantages.



448

449 **Figure 5.**

450 Partial wavelet coherency (PWC) between evaporation (E) and relative humidity (RH) after  
 451 excluding the effect of mean temperature (T) using the classical implementation (Eq. 15)  
 452 (a) and differences in PWC between the new (Eq.14) and classical implementation as a  
 453 function of scale (b).

454 Compared with the Mihanović et al. (2009) method, the additional phase information

455 from the new PWC is another advantage of this new method. This is because phase  
456 information is directly related to the type of correlation, i.e., in-phase and out-of-phase  
457 indicating positive and negative correlation, respectively. Different types of correlations  
458 were usually found at different locations and scales (Hu et al., 2017b). The phase  
459 information helps understand the differences in associated mechanisms or processes at  
460 different locations and scales. In addition, the phase information will allow us to detect the  
461 changes in not only the degree of correlation (i.e., coherence) but also the type of correlation  
462 after excluding the effect of other variables. For example, E and RH were positively  
463 correlated at the 1-year cycle (8–16 months) from year 1979 to 1995. This is because higher  
464 evaporation usually occurs in summer when high T coincides with high RH as influenced  
465 by the monsoon climate in the study area (Fig. S4 of Sect. S3 in the Supplement).  
466 Interestingly, after excluding the effect of T, E was negatively correlated with RH at the  
467 scale of 1 year as we expect (Fig. 3d).

468 Moreover, our new PWC method applies to cases with more than one excluding variable,  
469 which is a knowledge gap. When multiple variables are correlated with both the predictor  
470 and response variables, the correlations between predictor and response variables may be  
471 misleading if the effects of all these multiple variables were not removed. For example, at  
472 the dominant scale (i.e., 1 year) of E variation, contrasting effects of RH on E existed after  
473 excluding the effects of T (negative) or SH (positive) (Fig. 3d-e). However, after the effects  
474 of all other variables were excluded, there were negligible effects of RH on E at this scale  
475 (Fig. 4b). In this case, the relationship between E and RH at the scale of 1 year can be  
476 misleading after removing the effects of only one variable. In addition, the dominant role

477 of mean temperature in driving free water evaporation at the 1-year cycle was proved by  
478 removing the effects of all other meteorological factors (Fig. 4a). This also further verifies  
479 the suitability of the Hargreaves model (only air temperature and incident solar radiation  
480 required) (Hargreaves, 1989) for estimating potential evapotranspiration on the Chinese  
481 Loess Plateau (Li, 2012).

## 482 **5.2 Weaknesses**

483 The new method has the risk to produce spurious high correlations after excluding the  
484 effect from other variables. Take the artificial dataset for example, at the scale of 32, PWC  
485 values between  $y$  and  $y_2$  after excluding  $y_4$  are not significant, but relatively high, partly  
486 because of small octaves per scale (octave refers to the scaled distance between two scales  
487 with one scale being twice or half of the other, default of 1/12). This spurious unexpected  
488 high PWC is caused by low values in both the numerator (partly associated with the low  
489 coherence between response  $y$  and predictor variables  $y_2$  at the scale of 32) and denominator  
490 (partly associated with the high coherence between response  $y$  and excluding variable  $y_4$  at  
491 the scale of 32) in Eq. (9). The same problem also exists in the classical implementation  
492 (Fig. S5 of Sect. S3 in the Supplement). So, caution should be taken to interpret those results.  
493 However, it seems that the domain with spurious correlation calculated by the new method  
494 is very limited and it is located mainly outside of the cones of influence. Moreover, the  
495 unexpected results can be easily ruled out with knowledge of BWC between response and  
496 predictor variables. It is expected that the correlation between two variables should not  
497 increase after excluding one or more variables. Therefore, BWC analysis is suggested for

498 better interpretation of the PWC results.

499 Similar to BWC and MWC, the confidence level of PWC calculated from the Monte  
500 Carlo simulation is based on a single hypothesis testing. But in reality, the confidence level  
501 of PWC values at all locations and scales needs to be tested simultaneously. Therefore, the  
502 significance test has the problem of multiple testing, i.e., more than one individual  
503 hypothesis is tested simultaneously (Schaepli et al., 2007; Schulte et al., 2015). The new  
504 method may benefit from a better statistical significance testing method. Options for  
505 multiple testing can be the Bonferroni adjusted  $p$  test (Westfall and Young, 1993) or false  
506 discovery rate (Abramovich and Benjamini, 1996; Shen et al., 2002), which is less stringent  
507 than the former. The AR(1) model was used to generate noise series for testing the  
508 confidence level of PWC. High-order autoregressive models rather than AR(1) may be  
509 beneficial for a significance test where spatial data (or time series) are characterized by  
510 long-range dependence (Szolgayová et al., 2014).

## 511 **6. Conclusions**

512 Partial wavelet coherency (PWC) is improved to investigate scale-specific and localized  
513 bivariate relationships after excluding the effect of one or more variables in geoscience.  
514 Method tests using stationary and non-stationary artificial datasets verified the known  
515 scale- and localized bivariate relationships after eliminating the effects of other variables.  
516 Compared with the previous PWC method, the new PWC method has the advantage of  
517 dealing with more than one excluding variable and providing the phase information (i.e.,  
518 correlation type) associated with PWC. In the case of one excluding variable, the PWC

519 implementation provided here (in the paper and the published code) produces more accurate  
520 coherence than the previously published PWC implementation that considered wrongly real  
521 coherence rather than complex coherence between every two variables. Application of the  
522 new method to the real dataset has further proved its robustness in untangling the bivariate  
523 relationships after removing the effects of all other variables in multiple location-scale  
524 domains. The new method provides a much needed data-driven tool for unraveling  
525 underlying mechanisms in both temporal and spatial data. Thus, combining with wavelet  
526 transform, BWC, and MWC, the new PWC method can be used to analyze various  
527 processes in geoscience, such as stream flow, droughts, greenhouse gas emissions (e.g.,  
528 N<sub>2</sub>O, CO<sub>2</sub>, and CH<sub>4</sub>), atmospheric circulation, and oceanic processes (e.g., El Niño-  
529 Southern Oscillation).

#### 530 **Code/Data availability**

531 The Matlab codes for calculating PWC, along with the updated MWC codes, are freely  
532 accessible (<https://figshare.com/s/bc97956f43fe5734c784>). The codes are developed based  
533 on those provided by Aslak Grinsted (<http://www.glaciology.net/wavelet-coherence>). The  
534 meteorological dataset can be obtained from the China Meteorological Administration.

#### 535 **Author contributions**

536 WH wrote the paper, developed the Matlab code, and analyzed the data. Both authors  
537 conceived the study, interpreted the results, and revised the paper.

538 **Competing interests**

539 The authors declare that they have no conflict of interest.

540 **Acknowledgements**

541 The preparation of this manuscript was supported by The New Zealand Institute for Plant  
542 and Food Research Limited under the Sustainable Agro-ecosystems programme.

543 **References**

544 Abramovich, F. and Benjamini, Y.: Adaptive thresholding of wavelet coefficients,  
545 Computational Statistics & Data Analysis, 22, 351-361, 1996.

546 Aloui, C., Hkiri, B., Hammoudeh, S., and Shahbaz, M.: A multiple and partial wavelet  
547 analysis of the oil price, inflation, exchange rate, and economic growth nexus in Saudi  
548 Arabia, Emerging Markets Finance and Trade, 54, 935-956, 2018.

549 Altarturi, B. H., Alshammari, A. A., Saiti, B., and Erol, T.: A three-way analysis of the  
550 relationship between the USD value and the prices of oil and gold: A wavelet analysis,  
551 AIMS Energy, 6, 487, 2018a.

552 Altarturi, B. H. M., Alshammari, A. A., Saiti, B., and Erol, T.: A three-way analysis of the  
553 relationship between the USD value and the prices of oil and gold: A wavelet analysis, Aims  
554 Energy, 6, 487-504, 2018b.

555 Biswas, A. and Si, B. C.: Identifying scale specific controls of soil water storage in a  
556 hummocky landscape using wavelet coherency, Geoderma, 165, 50-59, 2011.

557 Centeno, L. N., Hu, W., Timm, L. C., She, D. L., Ferreira, A. D., Barros, W. S., Beskow, S.,

558 and Caldeira, T. L.: Dominant Control of Macroporosity on Saturated Soil Hydraulic  
559 Conductivity at Multiple Scales and Locations Revealed by Wavelet Analyses, *Journal of*  
560 *Soil Science and Plant Nutrition*, 20, 2020.

561 Das, N. N. and Mohanty, B. P.: Temporal dynamics of PSR-based soil moisture across  
562 spatial scales in an agricultural landscape during SMEX02: A wavelet approach, *Remote*  
563 *Sensing of Environment*, 112, 522-534, 2008.

564 Graf, A., Bogena, H. R., Drüe, C., Hardelauf, H., Pütz, T., Heinemann, G., and Vereecken,  
565 H.: Spatiotemporal relations between water budget components and soil water content in a  
566 forested tributary catchment, *Water Resour Res*, 50, 4837-4857, 2014.

567 Grinsted, A., Moore, J. C., and Jevrejeva, S.: Application of the cross wavelet transform  
568 and wavelet coherence to geophysical time series, *Nonlinear Processes in Geophysics*, 11,  
569 561-566, 2004.

570 Gu, X. F., Sun, H. G., Tick, G. R., Lu, Y. H., Zhang, Y. K., Zhang, Y., and Schilling, K.:  
571 Identification and Scaling Behavior Assessment of the Dominant Hydrological Factors of  
572 Nitrate Concentrations in Streamflow, *J Hydrol Eng*, 25, 06020002, 2020.

573 Hargreaves, G. H.: Accuracy of estimated reference crop evapotranspiration, *Journal of*  
574 *irrigation and drainage engineering*, 115, 1000-1007, 1989.

575 Hu, W., Chau, H. W., Qiu, W. W., and Si, B. C.: Environmental controls on the spatial  
576 variability of soil water dynamics in a small watershed, *J Hydrol*, 551, 47-55, 2017a.

577 Hu, W. and Si, B. C.: Technical note: Multiple wavelet coherence for untangling scale-  
578 specific and localized multivariate relationships in geosciences, *Hydrol Earth Syst Sc*, 20,  
579 3183-3191, 2016.

580 Hu, W., Si, B. C., Biswas, A., and Chau, H. W.: Temporally stable patterns but seasonal  
581 dependent controls of soil water content: Evidence from wavelet analyses, *Hydrol Process*,  
582 31, 3697-3707, 2017b.

583 Jia, X., Zha, T., Gong, J., Zhang, Y., Wu, B., Qin, S., and Peltola, H.: Multi-scale dynamics  
584 and environmental controls on net ecosystem CO<sub>2</sub> exchange over a temperate semiarid  
585 shrubland, *Agricultural and Forest Meteorology*, 259, 250-259, 2018.

586 Kenney, J. F. and Keeping, E. S.: *Mayhematics of Statistics*, D. van Nostrand, 1939.

587 Koopmans, L. H.: *The spectral analysis of time series*, Elsevier, 1995.

588 Lakshmi, V., Piechota, T., Narayan, U., and Tang, C.: Soil moisture as an indicator of  
589 weather extremes, *Geophysical research letters*, 31, L11401, 2004.

590 Li, H., Dai, S., Ouyang, Z., Xie, X., Guo, H., Gu, C., Xiao, X., Ge, Z., Peng, C., and Zhao,  
591 B.: Multi-scale temporal variation of methane flux and its controls in a subtropical tidal salt  
592 marsh in eastern China, *Biogeochemistry*, 137, 163-179, 2018.

593 Li, Z.: Applicability of simple estimating method for reference crop evapotranspiration in  
594 Loess Plateau, *Transactions of the Chinese Society of Agricultural Engineering*, 28, 106-  
595 111, 2012.

596 Mares, I., Mares, C., Dobrica, V., and Demetrescu, C.: Comparative study of statistical  
597 methods to identify a predictor for discharge at Orsova in the Lower Danube Basin,  
598 *Hydrological Sciences Journal*, 65, 371-386, 2020.

599 Mihanović, H., Orlić, M., and Pasarić, Z.: Diurnal thermocline oscillations driven by tidal  
600 flow around an island in the Middle Adriatic, *Journal of Marine Systems*, 78, S157-S168,  
601 2009.



602 Mutascu, M. and Sokic, A.: Trade openness-CO<sub>2</sub> emissions nexus: a wavelet evidence from  
603 EU, *Environmental Modeling & Assessment*, 25, 1-18, 2020.

604 Nalley, D., Adamowski, J., Biswas, A., Gharabaghi, B., and Hu, W.: A multiscale and  
605 multivariate analysis of precipitation and streamflow variability in relation to ENSO, NAO  
606 and PDO, *J Hydrol*, 574, 288-307, 2019.

607 Ng, E. K. and Chan, J. C.: Geophysical applications of partial wavelet coherence and  
608 multiple wavelet coherence, *Journal of Atmospheric and Oceanic Technology*, 29, 1845-  
609 1853, 2012a.

610 Ng, E. K. and Chan, J. C.: Interannual variations of tropical cyclone activity over the north  
611 Indian Ocean, *International Journal of Climatology*, 32, 819-830, 2012b.

612 Polansky, L., Wittemyer, G., Cross, P. C., Tambling, C. J., and Getz, W. M.: From moonlight  
613 to movement and synchronized randomness: Fourier and wavelet analyses of animal  
614 location time series data, *Ecology*, 91, 1506-1518, 2010.

615 Rathinasamy, M., Agarwal, A., Parmar, V., Khosa, R., and Bairwa, A.: Partial wavelet  
616 coherence analysis for understanding the standalone relationship between Indian  
617 Precipitation and Teleconnection patterns, arXiv preprint arXiv:1702.06568, 2017. 2017.

618 Schaefli, B., Maraun, D., and Holschneider, M.: What drives high flow events in the Swiss  
619 Alps? Recent developments in wavelet spectral analysis and their application to hydrology,  
620 *Adv Water Resour*, 30, 2511-2525, 2007.

621 Schulte, J., Duffy, C., and Najjar, R.: Geometric and topological approaches to significance  
622 testing in wavelet analysis, *Nonlinear Processes in Geophysics*, 22, 2015.

623 Sen, A., Chaudhury, P., and Dutta, K.: On the co-movement of crude, gold prices and stock

624 index in Indian market, arXiv preprint arXiv:1904.05317, 2019. 2019.

625 Shen, X., Huang, H.-C., and Cressie, N.: Nonparametric hypothesis testing for a spatial  
626 signal, *Journal of the American Statistical Association*, 97, 1122-1140, 2002.

627 Si, B. C.: Spatial scaling analyses of soil physical properties: A review of spectral and  
628 wavelet methods, *Vadose Zone Journal*, 7, 547-562, 2008.

629 Si, B. C. and Farrell, R. E.: Scale-dependent relationship between wheat yield and  
630 topographic indices: A wavelet approach, *Soil Sci Soc Am J*, 68, 577-587, 2004.

631 Si, B. C. and Zeleke, T. B.: Wavelet coherency analysis to relate saturated hydraulic  
632 properties to soil physical properties, *Water Resour Res*, 41, W11424, 2005.

633 Song, X. M., Zhang, C. H., Zhang, J. Y., Zou, X. J., Mo, Y. C., and Tian, Y. M.: Potential  
634 linkages of precipitation extremes in Beijing-Tianjin-Hebei region, China, with large-scale  
635 climate patterns using wavelet-based approaches, *Theoretical and Applied Climatology*,  
636 141, 1251-1269, 2020.

637 Su, L., Miao, C., Duan, Q., Lei, X., and Li, H.: Multiple - wavelet coherence of world's  
638 large rivers with meteorological factors and ocean signals, *Journal of Geophysical Research:*  
639 *Atmospheres*, 124, 4932-4954, 2019.

640 Szolgayová, E., Arlt, J., Blöschl, G., and Szolgay, J.: Wavelet based deseasonalization for  
641 modelling and forecasting of daily discharge series considering long range dependence, *J*  
642 *Hydrol Hydromech*, 62, 24-32, 2014.

643 Tan, X., Gan, T. Y., and Shao, D.: Wavelet analysis of precipitation extremes over Canadian  
644 ecoregions and teleconnections to large - scale climate anomalies, *Journal of Geophysical*  
645 *Research: Atmospheres*, 121, 14469-14486, 2016.

646 Torrence, C. and Compo, G. P.: A practical guide to wavelet analysis, *Bulletin of the*  
647 *American Meteorological society*, 79, 61-78, 1998.

648 Wendroth, O., Alomran, A. M., Kirda, C., Reichardt, K., and Nielsen, D. R.: State-Space  
649 Approach to Spatial Variability of Crop Yield, *Soil Sci Soc Am J*, 56, 801-807, 1992.

650 Westfall, P. H. and Young, S. S.: Resampling-based multiple testing: Examples and methods  
651 for p-value adjustment, John Wiley & Sons, 1993.

652 Wu, K., Zhu, J., Xu, M., and Yang, L.: Can crude oil drive the co-movement in the  
653 international stock market? Evidence from partial wavelet coherence analysis, *The North*  
654 *American Journal of Economics and Finance*, 2020. 101194, 2020.

655 Yan, R. and Gao, R. X.: A tour of the tour of the Hilbert-Huang transform: an empirical tool  
656 for signal analysis, *IEEE Instrumentation & Measurement Magazine*, 10, 40-45, 2007.

657 Zhao, R., Biswas, A., Zhou, Y., Zhou, Y., Shi, Z., and Li, H.: Identifying localized and scale-  
658 specific multivariate controls of soil organic matter variations using multiple wavelet  
659 coherence, *Sci Total Environ*, 643, 548-558, 2018.

660